Onset of a modulational instability in trapped dipolar Bose-Einstein condensates

Igor Ferrier-Barbut, Matthias Wenzel, Matthias Schmitt, Fabian Böttcher, and Tilman Pfau

5. Physikalisches Institut and Center for Integrated Quantum Science and Technology IQST, Universität Stuttgart, Pfaffenwaldring 57, 70550 Stuttgart, Germany

We explore the phase diagram of a finite-sized dysprosium dipolar Bose-Einstein condensate in a cylindrical harmonic trap. We monitor the final state after the scattering length is lowered from the repulsive BEC regime to the quantum droplet regime. Either an adiabatic transformation between a BEC and a quantum droplet is obtained or, above a critical trap aspect ratio $\lambda_c = 1.87(14)$, a modulational instability results in the formation of multiple droplets. This is in full agreement with the predicted structure of the phase diagram with a crossover region below λ_c and a multistable region above. Our results provide the missing piece connecting the previously explored regimes resulting in a single or multiple dipolar quantum droplets.

Ultracold dipolar gases constitute a new playground for exploring interaction effects in quantum fluids, in particular, because a natural intrinsic length scale emerges, stemming from the combined effects of an anisotropic long-range dipole-dipole interaction (DDI) and external forces. This fact, known to the realm of classical magnetic fluids (ferrofluids) for decades [1], has been understood to hold for dipolar Bose-Einstein condensates (DBECs) more recently. The first manifestations were theoretically predicted in finite-size, trapped DBECs: a structuring of the density profile [2–5]. In the thermodynamic limit, Ref. [6] predicted the appearance of a minimum in the dispersion relation of infinite "pancake"-shaped DBECs in the ground state of a harmonic trap. This minimum was called the roton minimum, inspired by a similar behavior of the dispersion relation in superfluid helium.

These features of the equilibrium many-body state of the quantum fluid were also found to alter its stability. In the infinite case, when changing the parameters (e.g., scattering length a for contact interactions, trapping strength), the roton minimum softens, and leads to an instability at finite wavelength [6]. In finite-size DBECs numerical simulations of the Gross-Pitaevskii equation with a DDI predicted the existence of an instability characterized by an ensemble of local collapses [7,8]. Such a collapse can be understood as the softening of a collective mode ($\omega^2 < 0$), which belongs to the discrete part of the spectrum where momentum k is not a good quantum number, such that $\eta = \langle k \rangle \times R_{\text{BEC}} \lesssim 1$ [9]. Here, R_{BEC} is the typical size of the BEC and $\langle k \rangle$ is taken for the given mode. The unstable mode differs from the lowest-lying surface and monopole modes. This leads to the appearance of multiple collapses rather than a global collapse. We will refer here both for the finite-size ($\eta \lesssim 1$) and thermodynamic limit ($\eta \gg 1$) to such instabilities as modulational instabilities. In contact-interacting BECs, a modulational instability has been recently reported at a negative scattering length [10,11]. The modulational instability of contact-interacting BECs differs from that of DBECs because all lowest-lying modes are unstable, and the favored wavelength for the instability is set to the mode that has the highest growth rate [10]. The observation

of such modulational instabilities in DBECs was reported for ^{164}Dy both in cylindrically symmetric [12] and elongated traps [13,14], in the finite-size limit $\eta \lesssim 1$. Recent experiments on erbium [15] report the observation of such an instability in the regime $\eta \gg 1$ of elongated DBECs, where it can be associated with the softening of a roton mode.

In the present work, we are interested in the regime $\eta \lesssim 1$, of harmonically trapped DBECs in cylindrical traps characterized by the aspect ratio $\lambda = \omega_z/\omega_r$, where $\omega_{r,z}$ denote trap frequencies and the magnetic field B is oriented along the z axis. We probe this with ^{164}Dy. The stability of DBECs as a function of λ and a was investigated first with ^{52}Cr BECs [16]. The dipolar length, defined by $a_{\text{dd}} = \frac{\mu_0 \mu^2 m}{12\pi \hbar^2}$, where m is the atom mass and μ the magnetic moment, is about eight times smaller for ^{52}Cr ($a_{\text{dd}} = 16a_0$) than for ^{164}Dy ($a_{\text{dd}} = 131a_0$). As a consequence, the modulational instability onset occurs for a much higher scattering length for Dy than Cr, and takes place even for much smaller samples. No direct evidence for its existence was reported with chromium. In the case of dysprosium, the absence of collapse following the modulational instabilities led to the discovery of quantum droplets stable only within beyond mean-field theory [13,17], observed also with an erbium DBEC [18] and in contact-interacting BEC mixtures [19–21].

The discovery of quantum droplets and the realization of the importance of beyond mean-field corrections [13] led to new recent works on the stability diagram [22,23]. The phase diagram as a function of λ and a can be calculated in the framework of the extended Gross-Pitaevskii equation (EGPE), which includes an effective term for the beyond mean-field correction; its approximations are discussed in Refs. [17,24]. One can then apply a Gaussian ansatz to the wave function which excludes density modulations, or resort to full simulations of the EGPE making no such restriction. The resulting diagram obtained with full simulations is represented in Fig. 1, and it contains different regions: At large a, a single solution exists, which is essentially a repulsive BEC with a cloud aspect ratio $\kappa = \sigma_r/\sigma_z$ close to that of the trap, weakly altered by magnetostriction. At a very low scattering length,
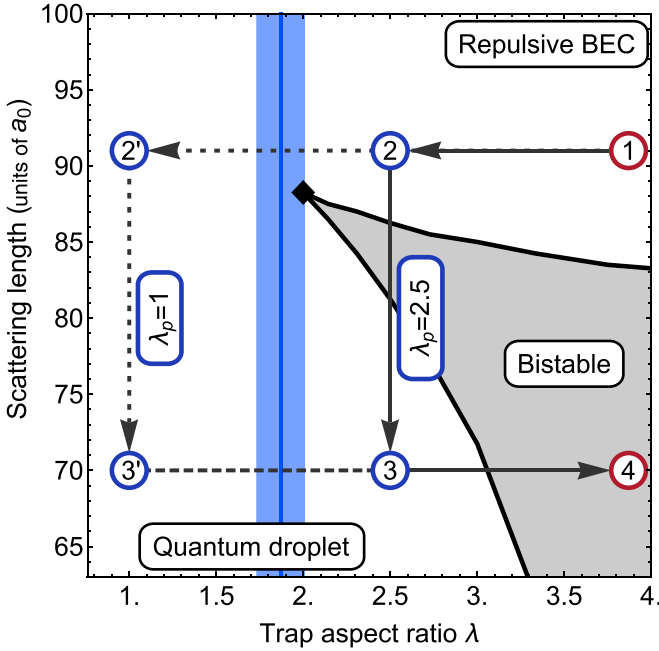
FIG. 1. Phase diagram for a cylindrically trapped ^{164}Dy BEC containing 6000 atoms, obtained with our experimental parameters: The z trapping frequency is fixed at $\omega_z = 2\pi \times 150$ Hz. The diagram is calculated with EGPE simulations. For λ below the critical point $\lambda < \lambda_c$ shown as a diamond, the repulsive BEC and the quantum droplet states are connected through a crossover. Above the critical point there is a multistable region where both are stable (shown in gray). Lowering the scattering length with λ above the critical point leads to a modulational instability. Our experimental procedure to locate the critical aspect ratio λ_c is shown as arrows, where we have assumed $a_{bg} = 70a_0$. We vary λ_p, and two indicative paths are shown [$\lambda_p = 2.5$ (through points 2 and 3) and $\lambda_p = 1.0$ (through points 2' and 3')]; timings are indicated in the text. The vertical blue line and blue area represent the resulting experimental value and error of $\lambda_c = 1.87(14)$ (see text).

a single solution exists, with an aspect ratio $\kappa \ll 1$ largely independent of λ. This solution corresponds to a quantum droplet that is stabilized by beyond mean-field corrections [13,22,23]. In between these two regions, and only for trap aspect ratios λ larger than a critical value λ_c, a bistable region exists, where both a repulsive $\kappa \gtrsim 1$ mean-field solution and a $\kappa \ll 1$ quantum droplet solution are stable. The critical point, shown as a black diamond, marks the transition between this bistable region and a region where the repulsive BEC and quantum droplets solutions are connected through a crossover. We find in the simulations the region boundaries as in Ref. [23], where the two local solutions are found by an imaginary time evolution using as the starting condition the ground state in the singly stable large a (small a) solution for the $\kappa \gtrsim 1$ ($\kappa \ll 1$) solution.

Then, the emergence of a modulational instability can be understood from this phase diagram. In the bistable region, the fact that a local minimum exists for a mean-field repulsive solution marks the fact that the lowest-lying modes of the system are not soft ($\omega^2 > 0$) since no global deformation can destabilize the gas. Therefore, by lowering a deep into the bistable region, one will observe a modulational instability

not taken into account in the Gaussian ansatz, triggered by a higher-lying mode. The authors of Ref. [22] suggested that by following a path in (λ, a) space that avoids the bistable region and lowers a in the crossover region $\lambda < \lambda_c$, one can prepare the quantum droplet ground state. A single quantum droplet was indeed observed by using $\lambda \ll 1$ with Er in Ref. [18]. Within the approximations of the extended Gross-Pitaevskii equation, this phase diagram can indeed be directly transposed to other atomic species with different a_{dd} such as Er, rescaling a and $\bar{\omega}$ to obtain the same values of ϵ_{dd} and $a/\sqrt{\hbar/m\bar{\omega}}$.

In our experiments we investigate the nature of the instability, as the scattering length is lowered, in cylindrically trapped ^{164}Dy DBECs as described above. We observe the onset of a modulational instability by varying the trap aspect ratio and obtain excellent agreement with theoretical predictions. For this, we implement a cylindrically symmetric harmonic trapping, with frequency ω_z along the dipoles and ω_r in the perpendicular plane. Our experiment is described in previous publications [12,17]. A three-beam optical dipole trap allows for a controllable aspect ratio $\lambda = \omega_z/\omega_r$. Using a Feshbach resonance located at $B_0 = 7.117(3)$ G with width $\Delta B = 51(15)$ mG, we are able to tune the scattering length above its background value a_{bg} [25].

Here, we restrict our exploration to aspect ratios $\lambda < 3$. For low enough a, the ground state of the system is a single quantum droplet [28]. However, depending on the path taken in phase space $\{\lambda, a\}$, we observe that the final state differs. If crossing the instability ($\lambda > \lambda_c$), one obtains an excited state, comprising several droplets. The final density distribution is shaped by postinstability nonlinear dynamics and does not allow one to study in depth the instability itself, for instance, identifying the unstable mode triggering the instability. But the observation of multiple droplets indicates that a modulational instability was crossed. If lowering a at $\lambda < \lambda_c$ in the crossover part of the phase diagram, then a single droplet should be obtained. To locate the onset of the modulational instability, we apply the following procedure, which is closely related to what is suggested in Ref. [22]: All our experiments start with a Bose-Einstein condensate of ≈ 6000 ^{164}Dy atoms, in a $\lambda_0 = 3.87(5)$ trap. The z trap frequency is kept constant $\omega_z = 2\pi \times 150(3)$ Hz while the radial one ω_r is varied to control λ. The initial scattering length is $a = 1.3(2)a_{bg}$ [at $B = 6.968(5)$ G] (point 1 in Fig. 1). The final point is fixed (point 4), with the same aspect ratio λ_0, but at a background scattering length within experimental uncertainty $a = 1.00(5)a_{bg}$ [$B = 5.468(5)$ G]. The path from the initial to final conditions is taken as follows, shown in Fig. 1: First (point 1 to 2), the trap aspect ratio is lowered in 50 ms to an arbitrary value $1.05 < \lambda_p \leqslant 2.55$. Second (point 2 to 3), the scattering length is lowered in 20 ms to the final value, and third, the aspect ratio is brought back in 50 ms to λ_0 (point 3 to 4). The only variable describing the path taken is thus λ_p. The mean trapping frequency varies between $\bar{\omega} = 2\pi \times 59$ Hz ($\lambda_p = 2.55$) and $\bar{\omega} = 2\pi \times 143$ Hz ($\lambda_p = 1.05$). The cloud is then immediately imaged *in situ* using phase-contrast imaging.

The final density distribution, shaped by beyond mean-field effects, retains a strong memory of the path taken, as visible in Fig. 2. For low aspect ratios, we observe a single droplet with little shot-to-shot variability, confirming expectations. This is independent of the aspect ratio up to a threshold. On the other
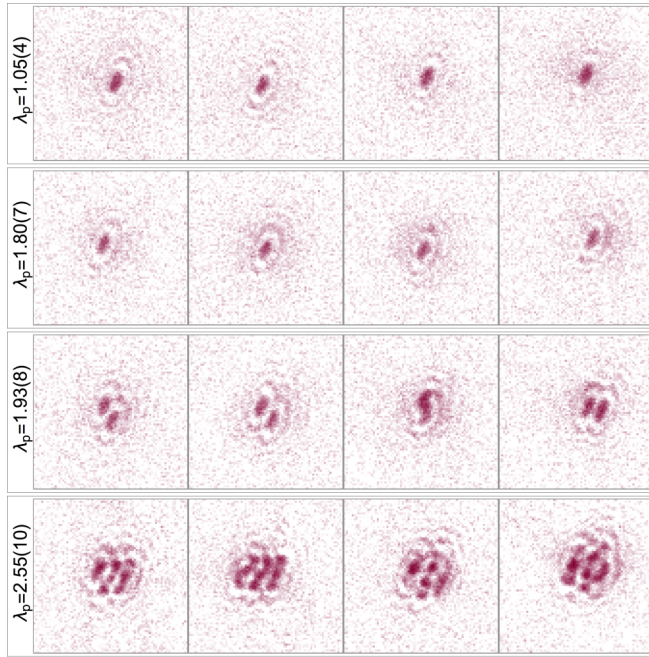
FIG. 2. Examples of final integrated density images resulting from different paths (identical within each row), indicated in the row. Imaging fringes are visible due to the size of the quantum droplet being smaller than our imaging resolution, and likely a slight displacement out of the focal plane. Misalignment of the objective caused a distortion of the images. The field of view in each image is $26\ \mu\text{m} \times 26\ \mu\text{m}$.

FIG. 3. (a)–(f) PCA image decomposition examples, comparing two different paths: (a)–(c) for $\lambda_\text{p} = 2.55(10)$ and (d)–(f) for $\lambda_\text{p} = 1.80(7)$. (a) and (d) Raw images. (b) and (e) Decomposition of the raw image only on the first five eigenvectors. The result for $\lambda_\text{p} = 1.80$ is very close to the raw image, while for $\lambda_\text{p} = 2.55$ it is markedly different. (c) and (f) Decomposition over 100 eigenvectors. The field of view in each image is $26\ \mu\text{m} \times 26\ \mu\text{m}$. (g) Comparing the average distribution of squared eigenvalues α_l^2 for four different paths. Below $\lambda_\text{p} \approx 1.9$ they are indistinguishable from each other, while above that value a clear difference is observed with more eigenvectors contributing.

hand, for large λ_p, the resulting density distribution is excited with several droplets that do not decay to the single droplet ground state, and the observed density shows a strong shot-to-shot variability.

To quantify this behavior, we apply a fit-free image analysis to the integrated density images. It is based on the principal component analysis (PCA) method [30]. PCA has been used to analyze experiments in ultracold atoms in the past (see, for instance, Refs. [31,32] and references therein). We apply it to our entire image data set $\{I_{k,s}\}$ ($k \in [1, N]$, $s \in [1, P]$). The set contains $N = 709$ images, each composed of $P = 80 \times 80$ pixels (chosen to give reasonable computational time). For this, we construct the correlation matrix $C_{mn} = \frac{1}{N}\sum_{k=1}^{N} \delta I_{k,m}\delta I_{k,n}$, where $\delta I_k = I_k - \langle I \rangle$ and $\langle I \rangle$ is the mean of all images. The individual images are then decomposed on the basis $\{v_l\}$ of eigenvectors of C: $\delta I_k = \sum_{l=1}^{N-1} \alpha_{l,k} v_l$ [33]. The components l are sorted by decreasing the eigenvalue η_l of C. This decomposition allows a quantitative comparison of the images. It holds a clear signature of the path taken, and provides a precise way to measure the critical aspect ratio λ_c.

Due to weak shot-to-shot fluctuations, in particular, in the center of mass visible in Fig. 2, each image k has a different $\{\alpha_l\}$ decomposition. Thus we plot the average distribution of $\langle \alpha_l^2 \rangle$ over all images taken after the same path. One indeed observes that it decays very differently depending on the path λ_p, as can be seen in Fig. 3. For low aspect ratios λ_p, the average distribution of eigenvalues $\langle \alpha_l^2 \rangle$ decays fast. Furthermore, the different distributions for different λ_p are indistinguishable
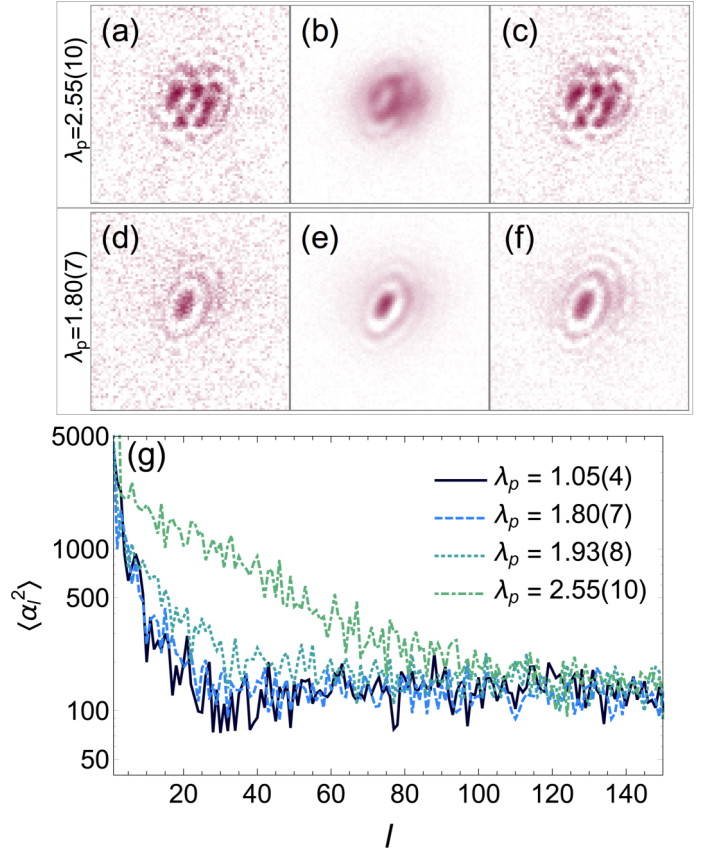
from each other. On the other hand, for large aspect ratios, this distribution decays much more slowly, and varies with λ_p.

Many observables using PCA can allow one to differentiate the images; we find that they all lead to the same conclusion, and we choose to calculate the quantity χ_k for image I_k defined as

$$\chi_k = \sum_{l=1}^{N-1}(\alpha_{l,k})^2 = \sum_{s=1}^{P}(\delta I_{k,s})^2. \tag{1}$$

The last identity shows that PCA decomposition is in fact not even necessary to obtain χ_k and that only a straightforward analysis can be done by simply taking the square of the image after having subtracted the mean of all images. Therefore this method measures how much each image differs from the overall mean; χ_k is of course increased when a large shot-to-shot variability occurs. Our analysis is thus similar to what was implemented, for instance, in Refs. [34,35]. However, the PCA decomposition was necessary to show that the $\langle \alpha_l^2 \rangle$ do not
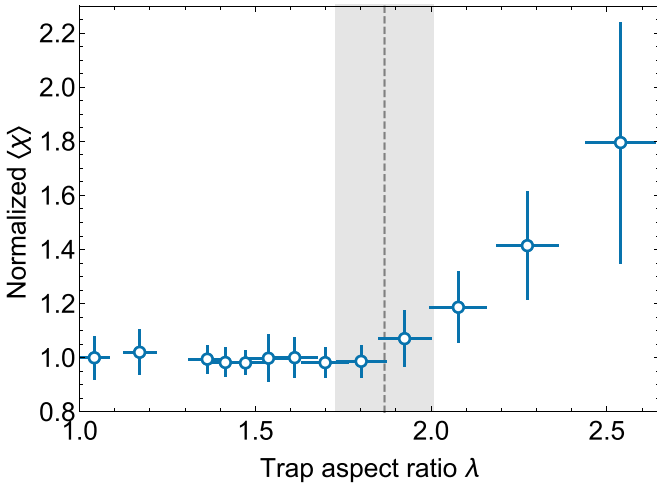
FIG. 4. $\langle\chi\rangle$ as a function of λ_p. The average is obtained from over 50 images for each λ_p, and the values are normalized to the lowest λ_p. The standard deviation of χ_k is shown as a vertical error bar. The gray area represents the confidence interval of the extracted λ_c.

differ from each other, and that one can indeed use only χ_k. In the PCA decomposition χ_k also reflects the "complexity" of the image I_k in the sense that the more eigenvectors need to be added and subtracted to reproduce the image, the higher is χ_k. We then calculate the average $\langle\chi\rangle$ again for all images obtained from the same path λ_p. The absolute value of $\langle\chi\rangle$ is arbitrary; it depends, for instance, on the number of atoms. Therefore we normalize it to the value obtained for the lowest $\lambda_p = 1.05$. The resulting normalized $\langle\chi\rangle$ as a function of λ_p is represented in Fig. 4. It exhibits a very clear threshold behavior, with unchanged $\langle\chi\rangle$ up to a critical value λ_c, followed by a linear increase above this threshold. The fact that below threshold the images do not differ significantly from each other while above threshold they vary strongly is thereby quantified. Then, from the data of Fig. 4, the critical aspect ratio can be extracted, and we observe that $\langle\chi\rangle$ departs from its background value at

$$\lambda_c = 1.87(14), \qquad (2)$$

with the confidence interval (gray area) given by the experimental uncertainty on λ. The exact λ_c value, represented as a blue area in Fig. 1, is in slightly better agreement with

predictions of the extended Gross-Pitaevskii equation with our experimental parameters ($\lambda_c = 2.0$, black diamond in Fig. 1) than expected using a Gaussian ansatz ($\lambda_c = 1.6$, not shown).

To conclude, our experiments start in a region where the repulsive Bose-Einstein condensate is stable. The fact that we are able to adiabatically prepare quantum droplets implies that when lowering λ at fixed a, no modulational instability is crossed. This means that the initial conditions are most likely in the single-solution repulsive BEC region as shown in Fig. 1. Given our uncertainty on the Feshbach resonance used to modulate the scattering length, our uncertainty in a is about 20 % in units of a_{bg}. In consequence, we obtain a weak lower bound on $a_{bg} \geqslant 58a_0$, in agreement with all expectations. Our final scattering length value is within the multistable region where within the Gaussian ansatz a repulsive BEC could be stable. Due to a modulational instability not taken into account within this theory, the BEC is unstable and forms multiple droplets. Thus, we have measured the experimental critical aspect ratio for the modulational instability of a dipolar Bose-Einstein condensate by a very straightforward data analysis involving no fit to the data. This provides the missing piece between the regimes explored in Ref. [12] ($\lambda \simeq 3$) and in Ref. [18] ($\lambda \simeq 0.1$), thus being a powerful confirmation of the structure of the phase diagram.

Locating this critical point is an important benchmark for all studies of harmonically trapped dipolar Bose-Einstein condensates; it allowed us to produce single self-bound droplets [24,36] which we reported in Ref. [17]. The natural continuation of our work is to locate the instability line as a function of λ and a above λ_c. This line cannot be theoretically predicted within the Gaussian ansatz. Experimentally, it will depend on other parameters such as temperature since thermal fluctuations might trigger the instability. Another direction is to understand the relationship between the modulational instabilities studied here and the soliton fragmentation reported for BEC mixtures in Ref. [37].

[1] R. E. Rosensweig, *Ferrohydrodynamics* (Courier Corporation, North Chelmsford, MA, 2013).

[2] K. Góral, K. Rzążewski, and T. Pfau, Bose-Einstein condensation with magnetic dipole-dipole forces, Phys. Rev. A **61**, 051601 (2000).

[3] K. Góral and L. Santos, Ground state and elementary excitations of single and binary Bose-Einstein condensates of trapped dipolar gases, Phys. Rev. A **66**, 023613 (2002).

[4] O. Dutta and P. Meystre, Ground-state structure and stability of dipolar condensates in anisotropic traps, Phys. Rev. A **75**, 053604 (2007).

[5] R. M. Wilson, S. Ronen, J. L. Bohn, and H. Pu, Manifestations of the Roton Mode in Dipolar Bose-Einstein Condensates, Phys. Rev. Lett. **100**, 245302 (2008).

[6] L. Santos, G. V. Shlyapnikov, and M. Lewenstein, Roton-Maxon Spectrum and Stability of Trapped Dipolar Bose-Einstein Condensates, Phys. Rev. Lett. **90**, 250403 (2003).

[7] N. G. Parker, C. Ticknor, A. M. Martin, and D. H. J. O'Dell, Structure formation during the collapse of a dipolar atomic Bose-Einstein condensate, Phys. Rev. A **79**, 013617 (2009).

[8] R. M. Wilson, S. Ronen, and J. L. Bohn, Angular collapse of dipolar Bose-Einstein condensates, Phys. Rev. A **80**, 023614 (2009).

[9] S. Ronen, D. C. E. Bortolotti, and J. L. Bohn, Radial and Angular Rotons in Trapped Dipolar Gases, Phys. Rev. Lett. **98**, 030406 (2007).

[10] J. H. V. Nguyen, D. Luo, and R. G. Hulet, Formation of matter-wave soliton trains by modulational instability, Science **356**, 422 (2017).

[11] P. J. Everitt, M. A. Sooriyabandara, M. Guasoni, P. B. Wigley, C. H. Wei, G. D. McDonald, K. S. Hardman, P. Manju, J. D. Close, C. C. N. Kuhn, S. S. Szigeti, Y. S. Kivshar, and N. P. Robins, Observation of modulational instability in Bose-Einstein condensates, Phys. Rev. A **96**, 041601(R) (2017).

[12] H. Kadau, M. Schmitt, M. Wenzel, C. Wink, T. Maier, I. Ferrier-Barbut, and T. Pfau, Observing the Rosensweig instability of a quantum ferrofluid, Nature (London) **530**, 194 (2016).

[13] I. Ferrier-Barbut, H. Kadau, M. Schmitt, M. Wenzel, and T. Pfau, Observation of Quantum Droplets in a Strongly Dipolar Bose Gas, Phys. Rev. Lett. **116**, 215301 (2016).

[14] I. Ferrier-Barbut, M. Schmitt, M. Wenzel, H. Kadau, and T. Pfau, Liquid quantum droplets of ultracold magnetic atoms, J. Phys. B **49**, 214004 (2016).

[15] L. Chomaz, R. M. W. van Bijnen, D. Petter, G. Faraoni, S. Baier, J. H. Becher, M. J. Mark, F. Waechtler, L. Santos, and F. Ferlaino, Observation of the roton mode in a dipolar quantum gas, arXiv:1705.06914.

[16] T. Koch, T. Lahaye, J. Metz, B. Frohlich, A. Griesmaier, and T. Pfau, Stabilization of a purely dipolar quantum gas against collapse, Nat. Phys. **4**, 218 (2008).

[17] M. Schmitt, M. Wenzel, F. Böttcher, I. Ferrier-Barbut, and T. Pfau, Self-bound droplets of a dilute magnetic quantum liquid, Nature (London) **539**, 259 (2016).

[18] L. Chomaz, S. Baier, D. Petter, M. J. Mark, F. Wächtler, L. Santos, and F. Ferlaino, Quantum-Fluctuation-Driven Crossover from a Dilute Bose-Einstein Condensate to a Macrodroplet in a Dipolar Quantum Fluid, Phys. Rev. X **6**, 041039 (2016).

[19] D. S. Petrov, Quantum Mechanical Stabilization of a Collapsing Bose-Bose Mixture, Phys. Rev. Lett. **115**, 155302 (2015).

[20] C. R. Cabrera, L. Tanzi, J. Sanz, B. Naylor, P. Thomas, P. Cheiney, and L. Tarruell, Quantum liquid droplets in a mixture of Bose-Einstein condensates, Science **359**, 301 (2018).

[21] G. Semeghini, G. Ferioli, L. Masi, C. Mazzinghi, L. Wolswijk, F. Minardi, M. Modugno, G. Modugno, M. Inguscio, and M. Fattori, Self-bound quantum droplets in atomic mixtures, arXiv:1710.10890.

[22] R. N. Bisset, R. M. Wilson, D. Baillie, and P. B. Blakie, Ground-state phase diagram of a dipolar condensate with quantum fluctuations, Phys. Rev. A **94**, 033619 (2016).

[23] F. Wächtler and L. Santos, Ground-state properties and elementary excitations of quantum droplets in dipolar Bose-Einstein condensates, Phys. Rev. A **94**, 043618 (2016).

[24] F. Wächtler and L. Santos, Quantum filaments in dipolar Bose-Einstein condensates, Phys. Rev. A **93**, 061603 (2016).

[25] The exact value of a_{bg} is still not fully known, with measurements in thermal gases reaching a value of $a_{bg} \simeq 90a_0$ [26,27] and a critical number measurement in self-bound droplets implying $a_{bg} \simeq 63a_0$ [17]. For the purpose of the present work, the exact a_{bg} is not directly relevant, as we will develop later.

[26] Y. Tang, A. Sykes, N. Q. Burdick, J. L. Bohn, and B. L. Lev, s-wave scattering lengths of the strongly dipolar bosons ^{162}Dy and ^{164}Dy, Phys. Rev. A **92**, 022703 (2015).

[27] T. Maier, I. Ferrier-Barbut, H. Kadau, M. Schmitt, M. Wenzel, C. Wink, T. Pfau, K. Jachymski, and P. S. Julienne, Broad universal Feshbach resonances in the chaotic spectrum of dysprosium atoms, Phys. Rev. A **92**, 060702 (2015).

[28] In another geometry with very confining traps, this is no longer the case [29].

[29] M. Wenzel, F. Böttcher, T. Langen, I. Ferrier-Barbut, and T. Pfau, Striped states in a many-body system of tilted dipoles, Phys. Rev. A **96**, 053630 (2017).

[30] I. T. Jolliffe, *Principal Component Analysis* (Springer, Berlin, 1986).

[31] S. R. Segal, Q. Diot, E. A. Cornell, A. A. Zozulya, and D. Z. Anderson, Revealing buried information: Statistical processing techniques for ultracold-gas image analysis, Phys. Rev. A **81**, 053601 (2010).

[32] R. Dubessy, C. D. Rossi, T. Badr, L. Longchambon, and H. Perrin, Imaging the collective excitations of an ultracold gas using statistical correlations, New J. Phys. **16**, 122001 (2014).

[33] Naively, since the dimension of C is $P \times P$, the sum would extend to $l = P$, but in fact given the definition of C, its rank is only N. The first component of the PCA decomposition is the data-set mean, which is here zero by definition of δI_k. Thus the sum can be stopped at $l = N - 1$.

[34] D. Chen, M. White, C. Borries, and B. DeMarco, Quantum Quench of an Atomic Mott Insulator, Phys. Rev. Lett. **106**, 235304 (2011).

[35] C. Meldgin, U. Ray, P. Russ, D. Chen, D. M. Ceperley, and B. DeMarco, Probing the Bose glass–superfluid transition using quantum quenches of disorder, Nat. Phys. **12**, 646 (2016).

[36] D. Baillie, R. M. Wilson, R. N. Bisset, and P. B. Blakie, Self-bound dipolar droplet: A localized matter wave in free space, Phys. Rev. A **94**, 021602 (2016).

[37] P. Cheiney, C. R. Cabrera, J. Sanz, B. Naylor, L. Tanzi, and L. Tarruell, Bright soliton to quantum droplet transition in a mixture of Bose-Einstein condensates, arXiv:1710.11079.